Thermo-mechanical behaviour of TRIP 1000 steel sheets subjected to low velocity perforation by conical projectiles at different temperatures

J.A. Rodríguez-Martínez [a,*], R. Pesci [b], A. Rusinek [c], A. Arias [a], R. Zaera [a], D.A. Pedroche [a]

[a] Department of Continuum Mechanics and Structural Analysis, University Carlos III of Madrid, Avda. de la Universidad 30, 28911 Leganés, Madrid, Spain
[b] ENSAM, Laboratory of Physics and Mechanics of Materials (LPMM), FRE CNRS 3236, 4 Rue Augustin Fresnel, 57078 Metz Cedex 3, France
[c] National Engineering School of Metz (ENIM), Laboratory of Mechanics, Biomechanics, Polymers and Structures (LaBPS), Ile du Saulcy, 57000 Metz, France

ABSTRACT

This paper presents and analyzes the behaviour of TRIP 1000 steel sheets subjected to low velocity perforation by conical projectiles. The relevance of this material resides in the potential transformation of retained *austenite* to *martensite* during impact loading. This process leads to an increase in strength and ductility of the material. However, this transformation takes place only under certain loading conditions strongly dependent on the initial temperature and deformation rate. In order to study the material behaviour under impact loading, perforation tests have been performed using a drop weight tower. Experiments were carried out at two different initial temperatures $T_0 = 213$ K and $T_0 = 288$ K, and within the range of impact velocities 2.5 m/s $\leqslant V_0 \leqslant$ 4.5 m/s. The experimental setup enabled the measuring of impact velocity, residual velocity, load time history and failure mode. In addition, dry and lubricated contacts between the striker and the plate have been investigated. Finally, by using X ray diffraction it has been shown that no *martensitic* transformation takes place during the perforation process. The causes involving the none appearance of *martensite* are examined.

1. Introduction

In the last decades, manufacturers have tried to minimize the production time and costs, while improving the properties and the quality of the products. This is also the case for important eco nomic sectors like the automobile, naval or civil industries, which have invested substantial efforts in developing new generations of steels for light weight structures capable of bearing strong mechan ical and thermo mechanical loading. In order to fulfil these objec tives, new alloys with high strength, ductility and toughness have been developed. Among them, the high strength TRIP steels (Trans formation Induced Plasticity) have become of great relevance.

These steels exhibit the transformation of *austenite* to *martens ite* under determined loading conditions. This transformation phe nomenon is desirable during impact loading since it increases the strength and ductility of the material retarding plastic localization as described by Curtze et al. (2009), Da Rocha and Silva de Oliveira (2009), Delannay et al. (2008), Fischer et al. (2000) and Jiménez et al. (2009).

According to Delannay et al. (2008), transformation of *austenite* into *martensite* can be triggered either by quenching or by loading the sample. Two effects are responsible for the deformation pro cess taking place in TRIP steels during and after the phase transfor

mation as shown by Delannay et al. (2008), Fischer et al. (2000) and Leblond et al. (1989):

- The "Magee effect" described by Magee (1966) is related to ori entation processes due to transformation of preferred variants.
- The "Greenwood Johnson effect" described by Greenwood and Johnson (1965) is related to the displacive character of the *austen ite martensite* transformation as discussed in Leblond et al. (1989). It corresponds to the plastic strain induced in the parent phase because of the volume difference between two coexisting phases.

The influence of plastic deformation, loading rate and initial temperature on the transformation kinetics of TRIP and dual phase steels has been analyzed by many researchers, for example Al Abbasi and Nemes (2003), Bouaziz and Guelton (2001), Bouaziz et al. (2008), Curtze et al. (2009), Huh et al. (2008), Iwamoto et al. (1998), Iwamoto and Tsuta (2000), Jiménez et al. (2009), Larour et al. (2006), Meftah et al. (2007), Papatriantafillou et al. (2006), Rodríguez Martínez et al. (2009) and Taleb and Petit (2006).

From these previous works several conclusions can be drawn:

- Plastic deformation triggers the *martensitic* transformation. It provides the driving force, (*corresponding to the difference in the free energy between austenite and martensite*) necessary to initiate and achieve the transformation.

* Corresponding author. Tel.:+34 91 624 8809; fax: +34 91 624 9430.
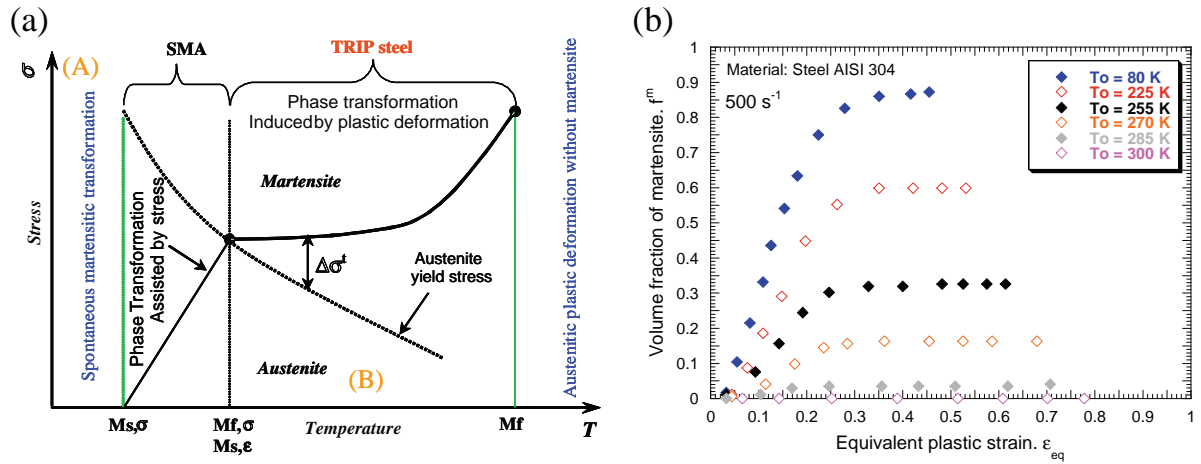*E-mail address:* jarmarti@ing.uc3m.es (J.A. Rodríguez-Martínez).

Fig. 1. (a) Schematic representation of the temperature effect on the martensitic transformation in TRIP steels. (b) Transformed volume fraction of martensite as a function of plastic strain in AISI 304 stainless steel, strain rate 500 s⁻¹ (Tomita and Iwamoto, 1995).

- *Martensitic* transformation is strongly dependent on the initial temperature as illustrated in the schematic drawing of Fig. 1a. The driving force required to induce the transformation varies with the temperature. For temperatures under a certain level M_s, the transformation may be reached in absence of plastic deformation. For temperatures above a critical value M_f, *martensite* will not be formed, no matter how much the *austenite* is deformed as reported by Lebedev and Kosarchuk (2000).
- Due to the relation existing between deformation and temperature in the material behaviour, the strain rate also plays a crucial role in the phase transformation process. For high strain rates, the *martensitic* transformation could not exist, Fig. 1b. Thermal softening of the material due to adiabatic heating under dynamic loading prevents the phase transformation.

Moreover, it is necessary to distinguish between two different types of TRIP steels:

- The high alloy TRIP steels (H TRIP) such as AISI 304, 301 or the high manganese steels. These *austenitic* steels contain large amounts of alloying elements such as Cr, Ni and/or Mn which stabilize the *austenite* as outlined by Fischer et al. (2000) and Liu et al. (2008).

- The low alloy TRIP steels (L TRIP) such as TRIP 600, 800, 1000 present a microstructure consisting of *ferrite*, *bainite* and retained *austenite* at room temperature. Generally, they contain small amounts of *austenite* stabilisers, which promotes the phase transformation as reported in Fischer et al. (2000) and Liu et al. (2008), Fig. 2.

Due to the different microstructures the transformation mechanisms are slightly different depending on the type of TRIP steel considered as described by Delannay et al. (2008) and Fischer et al. (2000).

In the present work, the attention will be focussed on the second type of TRIP steels previously mentioned. Generally, in L TRIP steels the retained *austenite* represents less than 20% of the total volume and only a fraction of *austenite* may transform during loading. These multiphase steels can be treated, in some measure, as composite materials, where the retained *austenite* acts as a second phase embedded in a *ferrite bainite* matrix. The transformation is basically controlled by the "Greenwood Johnson effect" as reported by Delannay et al. (2008). As a consequence of the *martensitic* transformation, strong local plasticity enhances strain hardening and global strain of the material. The L TRIP steel grades have major technological importance in comparison with the
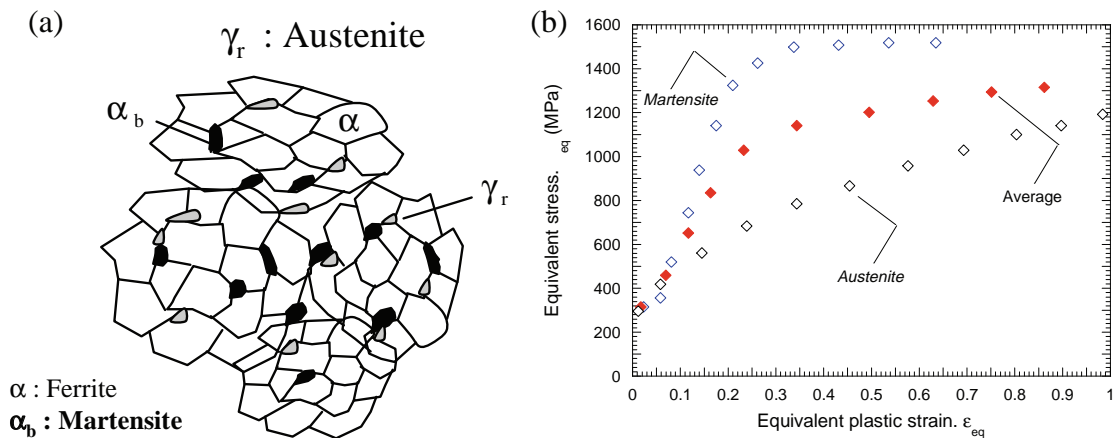

Fig. 2. (a) Sketch of the microstructure of a L-TRIP steel. (b) Stress–strain diagram showing the progressions of stress–strain curves of austenite, martensite and of an austenitic-martensitic microstructure (Iwamoto et al., 1998).

H TRIP grades. The main reason is the smaller amount of alloying elements, which will reduce their manufacturing costs.

Thus, the L TRIP steels are nowadays in widespread use in the automotive industry, for example in crash box structures, bumpers or side panels. These components are responsible for absorbing the kinetic energy during a crash or accident and may be subjected to dynamic loading during their service life. However, most of the works previously cited are restricted to the study of phase transformation phenomenon under quasi static loading. The transformation mechanisms under high strain rate have been rarely studied. The potential appearance of *martensitic* transformation under real service conditions is not clear in many cases.

In the present work, the main task is to carry out a comprehensive study on the behaviour of TRIP 1000 steel sheets subjected to low velocity perforation by conical projectiles. TRIP 1000 plates of $t = 1$ mm in thickness were tested using a drop weight tower. Experiments at different initial temperatures $T_0 = 213$ K and $T_0 = 288$ K and impact velocities 2.5 m/s $\leqslant V_0 \leqslant$ 4.5 m/s were carried out. Both dry and lubricated contacts between the projectile and the plate have been investigated. The applied loading conditions are assumed to be representative of those corresponding to the service conditions of many structural components used in engineering applications. The experimental setup allowed the measurement of the impact velocity, residual velocity, force time history and failure mode. The potential strain induced transformation during perforation has been evaluated using X ray diffraction (XRD). The procedure followed was to calculate the volume fraction of retained *austenite* in the plates, before testing, and when possible, after perforation. Thanks to this technique, it was possible to determine the residual stress state in *ferrite* in order to deduce and understand the behaviour of each phase and their role in the accommodation of plastic deformation during dynamic loading. The conducted analysis has led to a better understanding of the thermo viscoplastic behaviour of the TRIP 1000 steel and especially of the potential phase transformation under dynamic loading.

2. The multiphase TRIP 1000 steel

2.1. Microstructure and chemical composition

The material under investigation is a multiphase TRIP 1000 steel. Its chemical composition is given in Table 1 in accordance with the composition presented in Oliver et al. (2007).

The material underwent several heat treatments. After cold rolling, it first was annealed in the AC1 AC3 (*starting at AC*1 $\approx$ 1023 K and ending at AC3 $\approx$ 1113 K). The austenitization temperature range was chosen in order to obtain a maximum amount of retained *austenite*. Then, it was quickly cooled down to $T \approx 670$ K,

Table 1
Chemical composition of the TRIP 1000 steel (wt%) in accordance with the composition presented in Oliver et al. (2007).

C	Mn	Si	Cr	P	Al	Ni	Fe
0.16	1.58	1.47	0.20	0.087	0.048	0.04	Balance

when it underwent a tempering treatment for the formation of *bainite*. This process released the carbon from the *ferrite* to diffuse to the *austenite* (*carbon* enrichment and stabilization of the last phase). The resulting microstructure is a multiphased material constituted of *ferrite*, *bainite* and about 8% of retained *austenite.* Less than 2% on the surface and about 15% in the core was estimated. This gradient of composition through the thickness has been detected after a series of electropolishings every 50 μm reduction in thickness, Fig. 3. The volume fraction of each phase has been quantified using picture correlation techniques (SEM *investigations*) as well as XRD measurements (*see Section 3.2*).

Moreover, the *martensite* start temperature of this material, M_S=135 K, has been determined by dilatometry (*cooling rate of 20 °C/s*).

The surface roughness of the material has been analyzed. A mechanical treatment called *"Skin pass"* was applied to the TRIP 1000 steel during the manufacturing process. It generates micro plasticity on the surface of the specimen as illustrated in Fig. 4.

The induced local plasticity leads to the formation of plastic instabilities during loading. Using infrared camera recording, Lüder's band propagation was observed during the experiments performed in tension under quasi static loading as reported in Rusinek and Klepaczko (2009).

In addition, XRD enables to determine the initial textures in *ferrite* and *austenite* (*indicated* as conventional rolling textures as shown in Fig. 5) as well as the residual stress in the *ferritic* phase in the initial state of the plates: 25 MPa in the longitudinal direction (LD) and 70 MPa in the transverse direction (TD). These values of residual stresses are negligible in the case of a High Strength Steel (HSS) like TRIP 1000. Such reduced residual stress level has been induced by the previously mentioned mechanical treatment ("*skin pass*") which has been applied to the material after rolling.

In order to establish previous experimental observations, pole figures have been compared with those derived from a polycrystalline model reported by Pesci et al. (2009), Fig. 5. One thousand grains were considered, the crystallographic orientations of which were chosen at random (*many different orientations distribution*) so that no initial crystallographic texture was present. The textures are not perfectly identical, first because the simulation was finished after only 30% applied deformation. The second reason is that the diffraction goniometer could not collect the X ray data at $\Psi > 70°$.
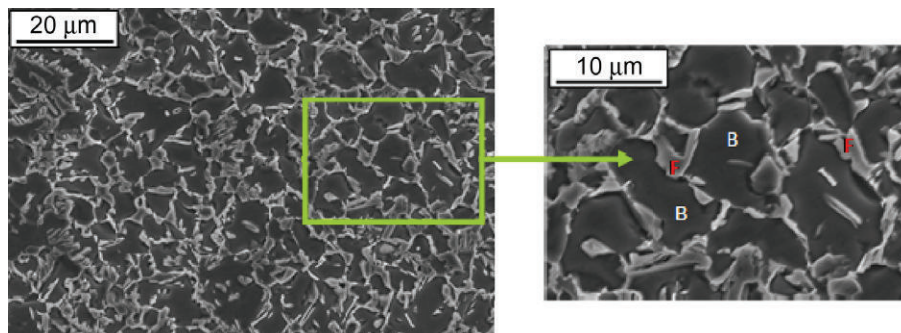

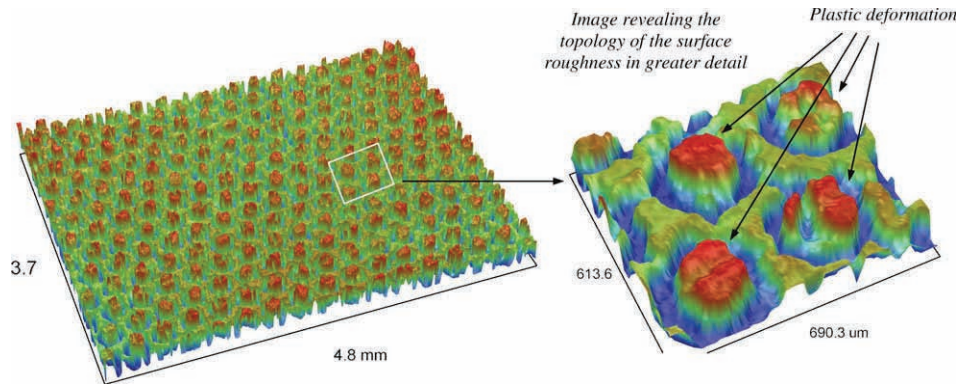**Fig. 3.** SEM micrograph of the steel TRIP 1000 showing mainly bainite (B) and ferrite (F) on the surface.
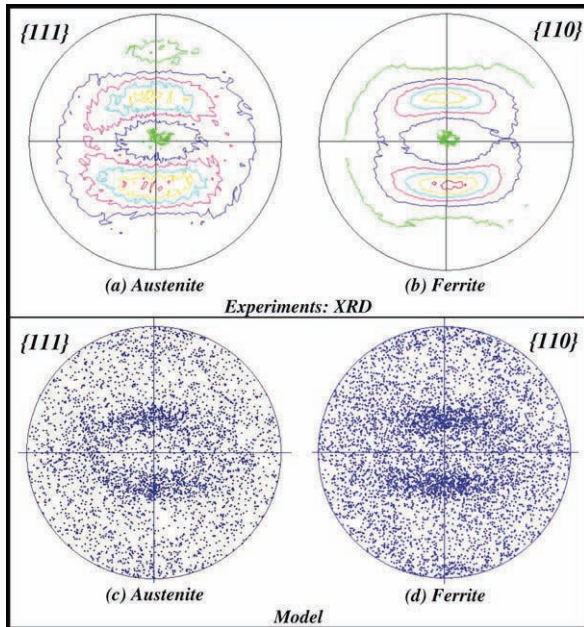
Fig. 4. Surface roughness of TRIP 1000 steel.

Fig. 5. (a)–(b) Recorded: FCC {1 1 1} and BCC {1 1 0} pole figures of austenite and ferrite by using XRD measurements. (c)–(d) Simulated: FCC {1 1 1} and BCC {1 1 0} pole figures corresponding to a rolling test: a polycrystalline microstructure of the measured sample section consisted of about 1000 grains per cm^2 was strained to 30%.

2.2. Thermo mechanical characterization

In order to characterize the mechanical behaviour of the mate rial, shear and tensile tests have been conducted at different load ing rates using a hydraulic machine as described in Rusinek and Klepaczko (2009). The evolution of the flow stress as a function of the plastic strain for different strain rates is shown in Fig. 6a. The TRIP 1000 steel shows a reduced strain rate sensitivity in the range of strain rates covered during the tests, Fig. 6a. Such an observation is in agreement with experimental data reported in the literature for other HSS as informed in Larour et al. (2007) and Rusinek et al. (2009a). Fig. 6b depicts how the strain rate sen sitivity parameter m decreases with increasing initial static yield stress.

Under quasi static loading, the material exhibits important temperature sensitivity as shown in Fig. 7a. Temperature decreas ing leads to an increasing in strain hardening, Fig. 7b. Such a behaviour seems to come from the deformation of *austenite* and subsequent *martensitic* transformation as proposed by Rusinek and Klepaczko (2009). Thus, temperature sensitivity is revealed as plastic strain dependent, Fig. 7c.

However, it has been noticed that *martensitic* transformation becomes limited with increasing loading rate due to the incipient heat generation inside the material as outlined by Rusinek and Klepaczko (2009). This is caused by two sources: *martensitic* trans formation and conversion of plastic work. This latter effect is emphasized by the deformation rate. At high strain rates the temperature sensitivity of TRIP steels is reduced and becomes
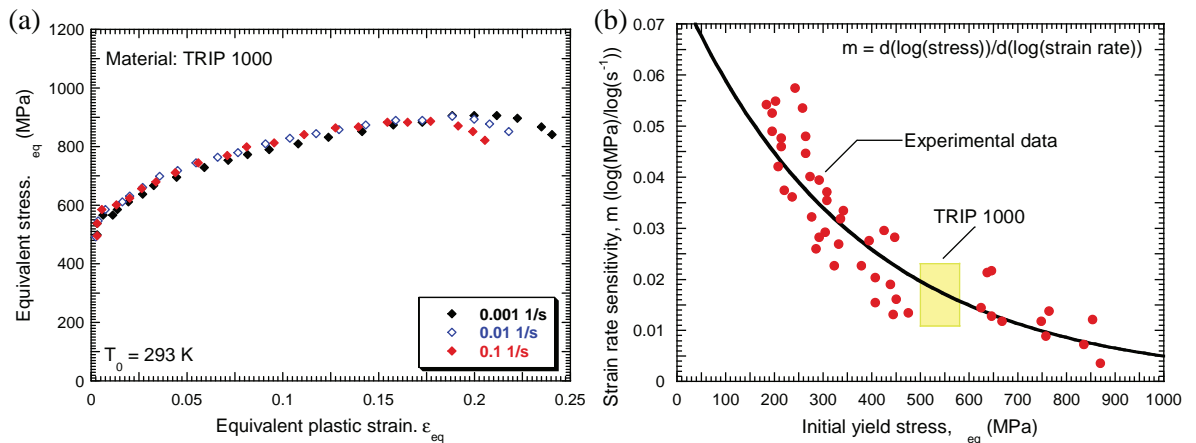

Fig. 6. (a) Flow stress of TRIP 1000 in dependence on the plastic strain for different loading rates. (b) Evolution of the strain rate sensitivity parameter as a function of the static initial yield stress for different steel alloys.
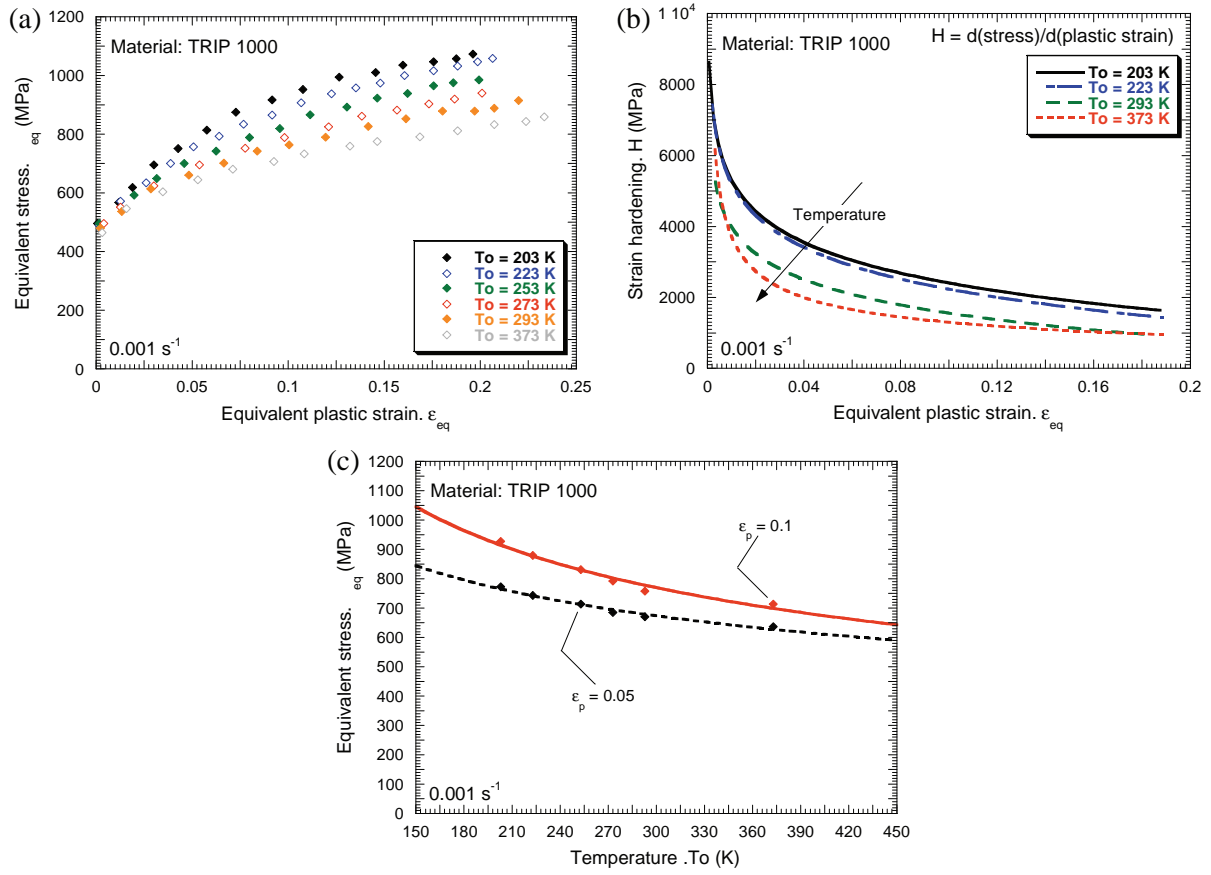
4

Fig. 7. (a) Flow stress of TRIP 1000 as a function of plastic strain for different initial temperatures. (b) Strain hardening of TRIP 1000 as a function of plastic strain for different initial temperatures. (c) Evolution of the flow stress as a function of temperature for different plastic strain values.
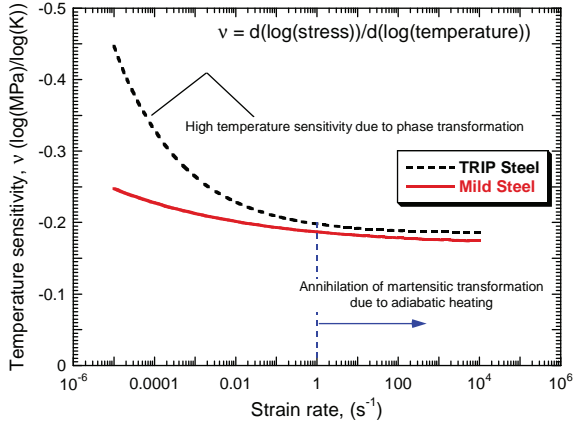

Fig. 8. Comparison of the temperature sensitivity for TRIP steel and mild steel.

comparable with the temperature sensitivity of plain carbon steels as shown by Rusinek and Klepaczko (2009), Fig. 8. It is clear that the reduction of the *martensitic* transformation is related to the increasing strain rate.

3. Experimental setups

In this section, the drop weight tower and the XRD technique will be introduced.

3.1. The drop weight tower

In order to conduct the perforation tests a drop weight tower has been used as described by Sanchez Saez et al. (2007) and illustrated in the schematic drawing of Fig. 9. This test allows a perpendicular impact on the TRIP steel sheets in a range of impact velocities varying from 2.5 m/s ⩽ V_0 ⩽ 4.5 m/s. Since the mass of the impactor may be chosen by the user, a wide range of impact energy can be achieved. The drop weight tower has a climatic chamber, allowing variations in the initial temperature during the tests of T_0 = 213 K and T_0 = 288 K, respectively. A thermocouple was connected to a temperature controller regulating the opening of an electrovalve. This allowed a controlled volume of liquid nitrogen to enter the chamber. Thus, the testing temperature could be accurately defined by the operator.

The tested square like specimens possess a size of A_t = 100 × 100 mm² and a thickness of h = 1 mm. They were clamped by screws all around the active surface of A_a = 80 × 80 mm². The screws were symmetrically fixed in order to avoid any disturbances during the test, Fig. 10. The device used to clamp the steel sheets had a transparent side made of PMMA. Such an arrangement allowed to film the perforation process using a high speed camera.

The steel striker used has a conical shape as shown in Fig. 11. Its larger diameter is $\varnothing_p$ = 20 mm and its mass is M_{imp} = 0.105 kg. After machining, the striker was oil quenched, thereby increasing the yield stress of the material up to $\sigma_y \approx 1.0$ GPa. It permitted to avoid its damage or erosion during perforation, Fig. 11.

The striker was attached to the instrumented bar of the drop weight tower, whose mass was M_{bar} = 0.761 kg. Additional mass
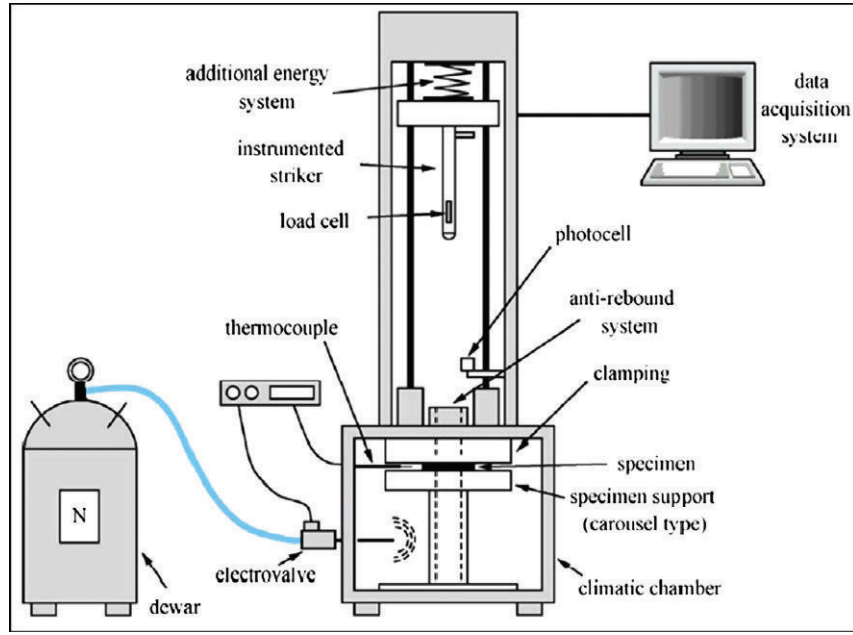
Fig. 9. Schematic representation of the drop weight tower.
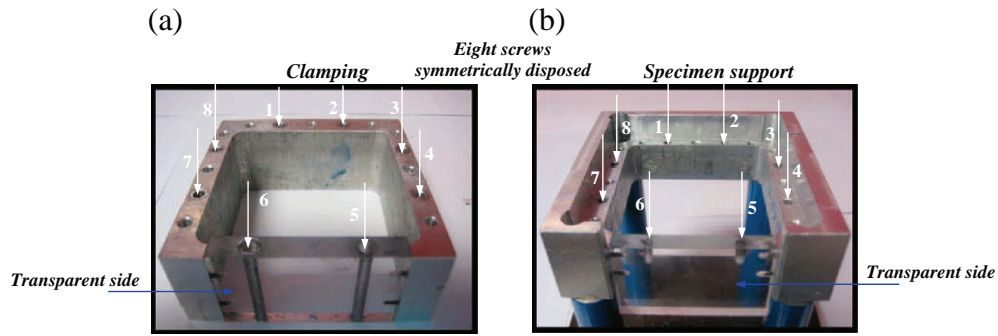
(a)   (b)

Fig. 10. Experimental device used to clamp the specimen in the perforation tests. (a) Clamping, (b) specimen support.

was added to the setup in order to increase the effective mass to M_{total} = 18.787 kg (*the range of the impact energy covers* 59 J $\leqslant E_i \leqslant$ 190 J). This additional mass would allow to complete the perfora tion of the steel sheets in the range of the impact velocities consid ered in this study. A load cell placed on the striker enabled to record the impact force versus time signal. The time dependent velocity and displacement of the striker during perforation can be quantified by integration of the impact force versus time curve. After the impact, an anti rebound system held the striker in order to avoid multi hits on the specimen if no perforation of the plate occurred.

According to the numerical estimations reported by Rodríguez Martínez et al. (2008) for similar impact configuration the maxi mum strain rate level is located on the cracking interfaces,

$\dot{\varepsilon}^p_{max} \approx 1000$ s ^{1}. Away from the cracking interfaces (*in the zone directly affected by the impact*), the strain rate level is assumed quite smaller, 10 s $^1 \leqslant \dot{\varepsilon}^p_{average} \leqslant$ 100 s ^{1}. These ranges of deformation rate are for guidance only. It is known that the strain rate in the target material is strongly dependent on the target zone as well as on the perforation stage.

3.2. The X ray diffraction technique

XRD has been used since it is a very efficient non destructive technique that enables to determine accurately the volume frac tion of each phase as well as the average stress state in the coexisting phases. Bragg's law provides the condition for a plane
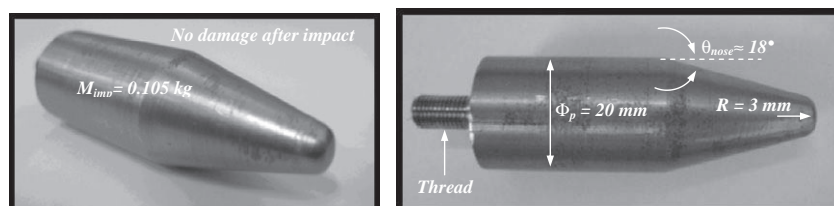

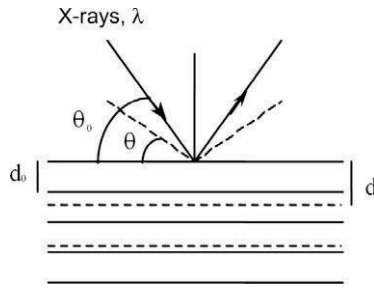**Fig. 11.** Conical striker used in the perforation tests.

Fig. 12. Principle of X-ray diffraction: d_0 and θ_0 are referring to the lattice spacing and to the Bragg angle corresponding to a free stress state; whereas d and θ are referring to the lattice spacing and to the Bragg angle under certain applied stress state.

Fig. 13. Portable PROTO goniometer used for XRD *measurements*.

wave to be diffracted by a set of lattice planes, as presented in the following equation:

$$2d_{hkl} \cdot \sin\theta = n\lambda \tag{1}$$

where d_{hkl} are the lattice plane spacings (*closest distance*) of a $\{hkl\}$ plane set, θ is the incident Bragg angle, λ is the wavelength of the incident X-ray beam and n is an integer corresponding to the order of reflection, as illustrated in the schematic drawing of Fig. 12. When Bragg's law is satisfied, diffraction occurs and peaks of scattered intensity can be observed.

First, the volume fraction of each phase has been calculated using a classic XRD analysis from the intensity of the diffraction peaks for both phases, *ferrite* and *austenite*. For the TRIP 1000 steel the amount cementite is very low ⩽1 vol% and the volume fraction of retained *austenite* can be obtained by using the following equation:

$$V_\gamma = 1/\left[1 + (I_\alpha/I_\gamma) \cdot (R_\gamma/R_\alpha)\right] \tag{2}$$

where I_α and I_γ are the intensities of the diffraction peaks of *ferrite* and *austenite*, respectively; R_α and R_γ are the coefficients depending on some parameters such as the absorption factor, the Lorentz polarisation factor, the multiplicity factor of the analysed $\{hkl\}$ planes, the volume of the crystal lattices and several others, see Hauk (1997). Furthermore, the sum of the partial volume fractions is equal to one, $V_\alpha + V_\gamma = 1$.

In TRIP steels *austenite* transforms to *martensite* during loading. The objective of the study was to determine the volume fraction of the transformed *martensite* in the impacted plates. The main problem of this technique is the difficulty in differentiating the *martensite* diffraction peaks from the *ferrite* ones, since these two phases have very similar lattice parameters. It was therefore impossible to detect the *martensite* and to quantify its volume fraction directly. However, since TRIP 1000 is a *martensite* free steel in its initial state, it was possible to carry out relevant analyses by calculating precisely the amount of *austenite* in the plates after testing. From this result the decrease in its volume fraction is associated to a similar volume fraction of *martensite*.

For a quantitative stress determination, the classical $\sin^2\psi$ method was used considering the lattice plane spacing d_{hkl} of a $\{hkl\}$ plane set as an internal strain gauge, as described by Hauk (1997) and Inal et al. (2006). Due to the complex geometry of the plates after testing, residual stresses have been determined on the surface of the specimens using a portable PROTO goniometer. This enables to analyze the shaped parts since the sample stays fixed during the whole analysis, (*the beam is moving around the specimen*), Fig. 13.

The most ductile phase in the material (*ferrite*) has been analyzed by using a chromium anticathode ($\lambda = 2.2897$ Å); in order

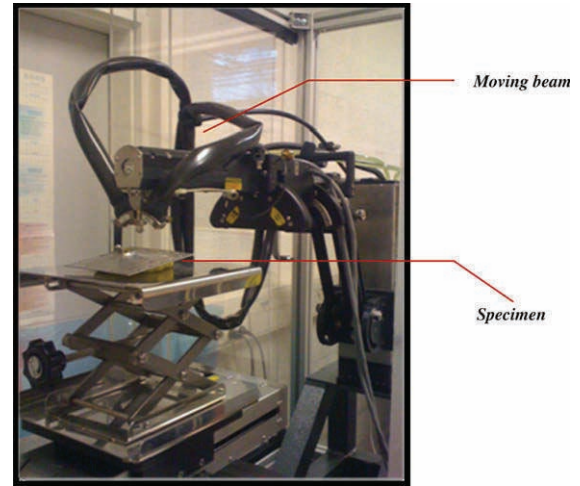to obtain optimum results (*best accuracy*), the analysis of the $\{211\}$ planes corresponding to a diffraction angle of $2\theta = 156.1°$ has been conducted. No measurements of residual stresses have been conducted in *austenite* because of the low volume fraction of this phase on the surface of the specimens. In order to obtain more precise values, synchrotron emission should be used to study the stress states in greater detail.

4. Influence of impact velocity, friction condition and initial temperature on the perforation process

In this section of the study, the effects of impact velocity, friction condition and initial temperature on the perforation process are analyzed. The effects of these parameters on the perforation of metallic sheets has been rarely studied, see Rusinek et al. (2009b), especially the influence of initial temperature was not studied in detail, mainly due to the complex experimental devices required for highly instrumented tests.

4.1. Effect of impact velocity

In order to estimate accurately the ballistic limit value, the residual velocity is compared to the initial velocity of the striker, Fig. 14. This residual velocity is assumed as the speed of the striker
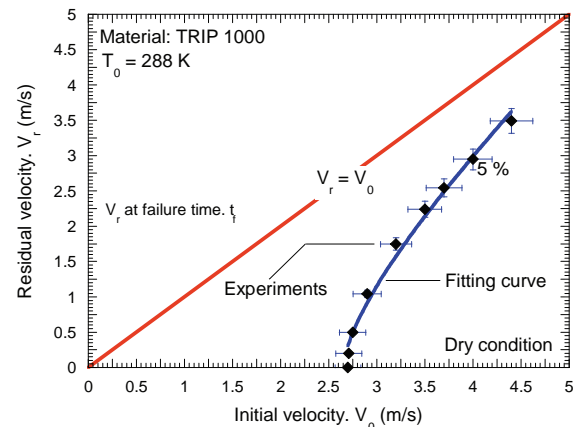

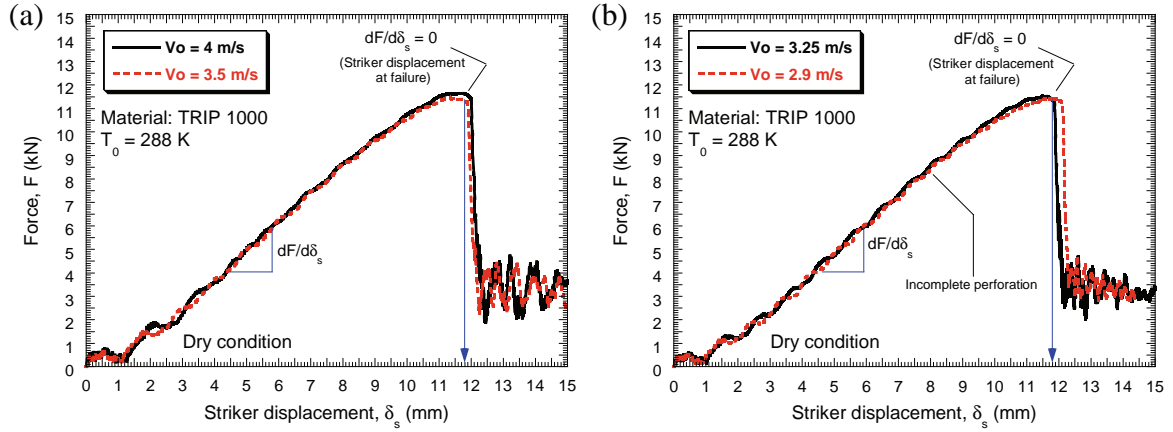**Fig. 14.** Residual velocity versus initial impact velocity at room temperature.

Fig. 15. Evolution of the force in dependence on the striker displacement for different impact velocities.
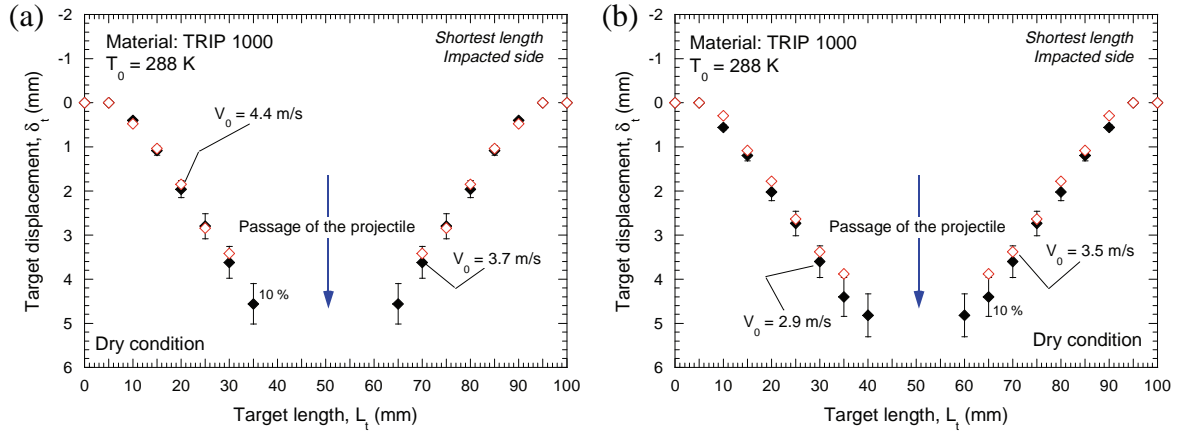

Fig. 16. Target displacement for different impact velocities.

corresponding to the failure time. This is considered as the time for which the projectile pierces the target and the ballistic limit is taken as the maximum speed of the striker for which no crack occurred in the target. The fitted data, as depicted in Fig. 14, exhi bit the characteristic shape of the curves obtained from perfora tion processes as outlined in greater detail in Arias et al. (2008), Borvik et al. (2002), Klepaczko et al. (2009) and Rusinek et al. (2008). The ballistic limit value obtained from the experiments performed at room temperature is $V_{bl} = 2.6$ m/s, as illustrated in Fig. 14.

For the range of impact velocities considered, the mechanisms involved in the perforation process do not vary with the initial velocity. The slope of the force/striker displacement curve (F δ_s) remains constant regardless the impact velocity, as shown in Fig. 15. The energy absorbed by the plate is almost unchanged.

The different behavior occurs for $V_0 \leqslant 3$ m/s. In such a case the perforation is incomplete because the entire striker did not pass through the target. The bending effect, determined on the shortest length of the target passing through the impact point and on the impacted side, is more accentuated and the energy absorbed by the plate in form of plastic work is slightly greater, as illustrated in Fig. 16.

The analysis of the post mortem specimens reveals that *petal ling* is the recurring failure mode for all perforation tests, as dem onstrated in Figs. 17 and 18. It has been noticed that neither the

rolling direction nor boundary conditions influence the initiation or the propagation of cracks.

A number of main petals occurring in each test varies between four and five, as shown in Figs. 17 and 18. This is consistent with the observations reported by Landkof and Goldsmith (1993) and Wierzbicki (1999). This number corresponds to a minimum of the total rate of energy dissipation. A larger number of petals would be expected for initial velocities out of the range of impact velocities applied in the present study as published in Rodríguez Martínez et al. (2008) and Rusinek et al. (2009b). For the impact velocities higher than a specific value, the energy lost by a projec tile quickly increases. This is a consequence of the influence of inertia in the mechanisms of perforation. The perforation process becomes less efficient.

Petalling is caused by the reduced thickness of the target and by the conical shape of the striker as discussed in Landkof and Gold smith (1993), Rodríguez Martínez et al. (2008), Rusinek et al. (2009b) and Wierzbicki (1999). In the initial stage of the impact the deformation is localized in the small area corresponding to the interface projectile/plate, as shown in Fig. 19a. That area of the target is strongly deformed and bent until failure occurs, Fig. 19b. When failure occurs, several small cracks are generated at the dome of the interface projectile/plate, as illustrated in Fig. 19c. Those cracks propagate until they reach the rear side of the plate due to the circumferential strain induced in the target by the passage of the projectile, as shown in Fig. 19d. As a conse
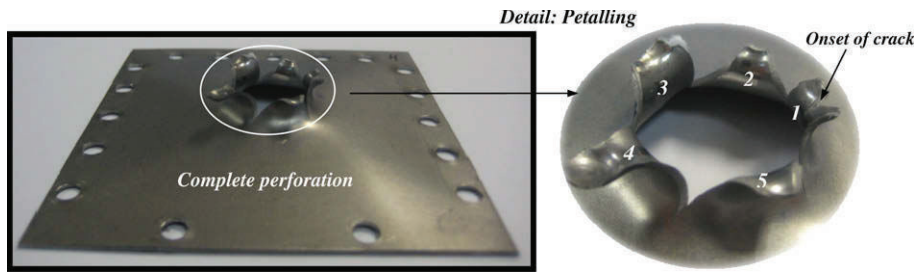
8

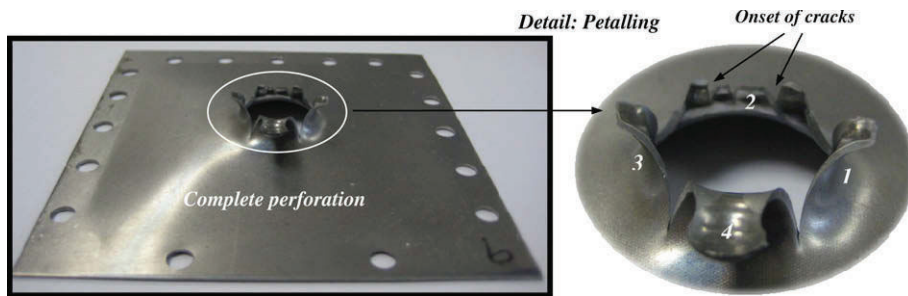**Fig. 17.** Petalling failure mode for V_0 = 4.4 m/s and T_0 = 288 K. Dry condition.

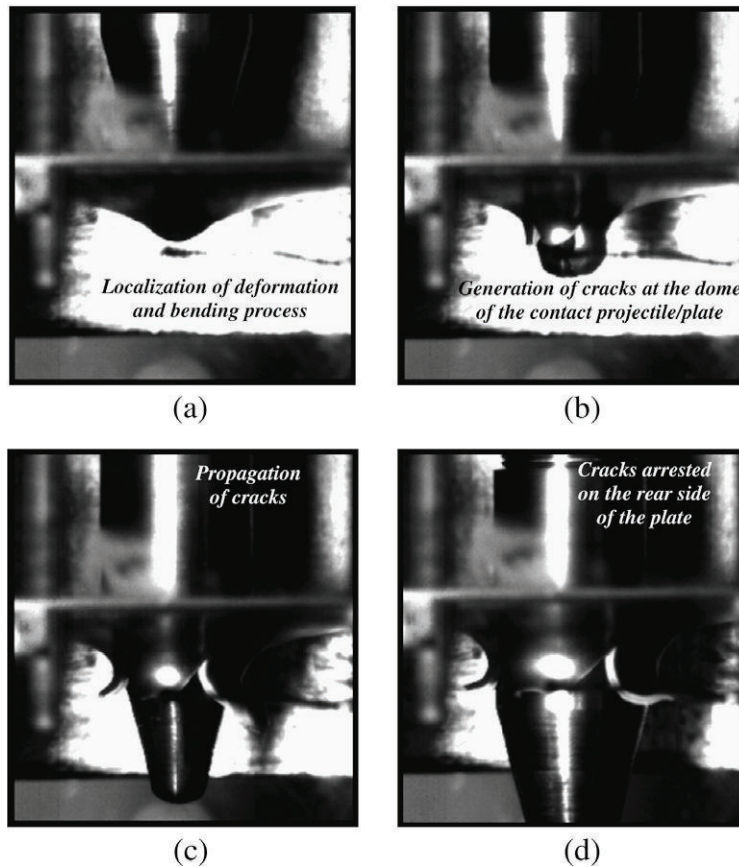**Fig. 18.** Petalling failure mode for V_0 = 3.5 m/s and T_0 = 288 K. Dry condition.

Fig. 19. Different stages of the perforation process for V_0 = 4.4 m/s and T_0 = 288 K. (a) Localization of deformation and bending process. (b) Formation of cracks at the dome of the contact projectile/plate. (c) Propagation of cracks. (d) Cracks arrested on the rear side of the plate.
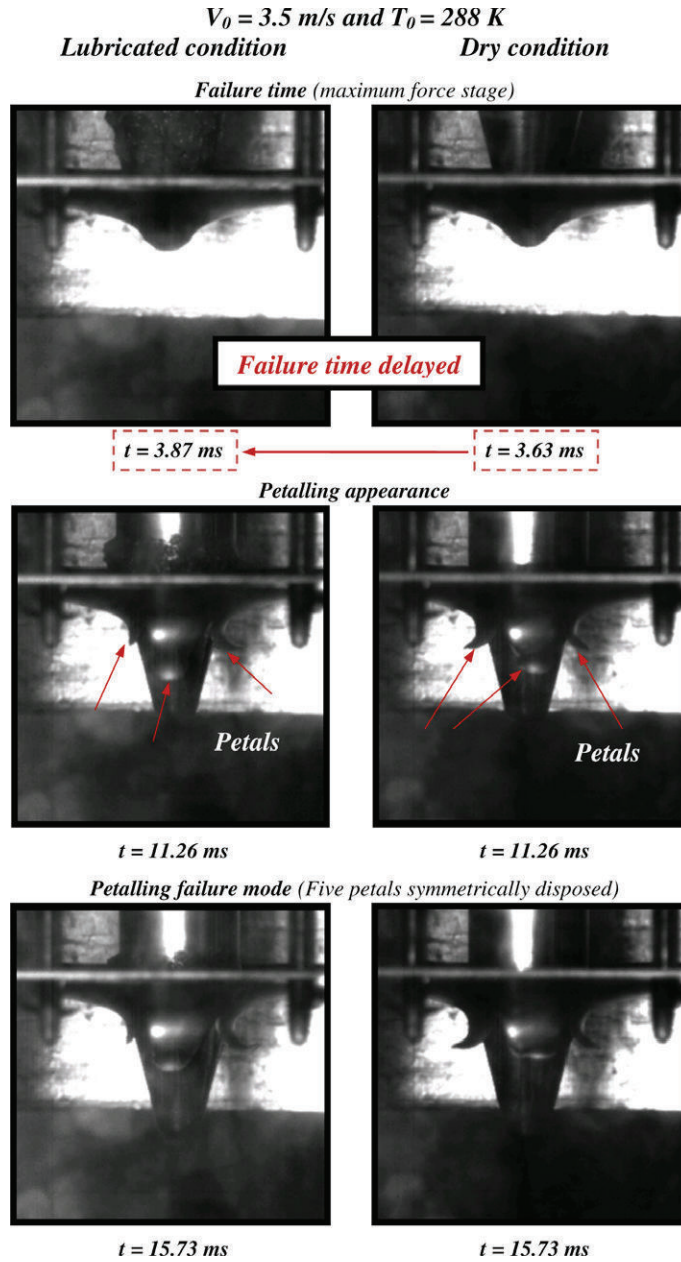
$V_0 = 3.5 \ m/s$ and $T_0 = 288 \ K$

Lubricated condition   **Dry condition**

Failure time (maximum force stage)

Failure time delayed

$t = 3.87 \ ms$ ← $t = 3.63 \ ms$

Petalling appearance

Petals   *Petals*

$t = 11.26 \ ms$ $t = 11.26 \ ms$

Petalling failure mode (Five petals symmetrically disposed)

$t = 15.73 \ ms$ $t = 15.73 \ ms$

Fig. 20. Perforation process of TRIP 1000 sheets under lubricated and dry conditions. $V_0 = 3.5$ m/s and $T_0 = 288$ K.

quence, several petals are formed, Figs. 18 and 19. These observations are in agreement with the experimental evidences and the numerical predictions reported by Landkof and Goldsmith (1993), Rodríguez Martínez et al. (2008), Rusinek et al. (2009b) and Wierzbicki (1999).

4.2. Effect of the projectile target friction

The effect of friction was evaluated using the technique previously reported by Rusinek et al. (2009b) in the case of ES steel plates subjected to perforation by hemispherical projectiles. Two friction conditions were considered: lubricated ($\mu \approx 0$) and dry ($\mu > 0$). In the case of the lubricated condition, several layers of grease and teflon are applied to the interface striker/plate.

It should be noted that the failure mode of the plates is not affected by the friction condition applied, as illustrated in Fig. 20.

Petalling is also the dominant failure mode taking place in all the tests conducted using lubricated contact, Fig. 20.

However, the perforation process shows some dependence on the type of contact. The evolution of force in relation to the striker displacement for both friction conditions and different impact velocities is depicted in Fig. 21. Both curves are superposed until the collapse of the target in the case of dry contact, as illustrated in Fig. 21. The target failure in the case of lubricated condition is delayed due to the absence of tangential stresses $\mu \approx 0$ on the interface striker/target, as shown in Fig. 22. The absence of tangential stresses reduces the localised deformation around the contact point striker/target. Radial sliding along the contact zone projectile/plate is longer in comparison with dry condition.

A larger striker displacement at failure time leads to a larger bending effect, Fig. 23. The difference in the permanent bending effect between both friction conditions becomes more noticeable as the impact velocity decreases, see Fig. 23.
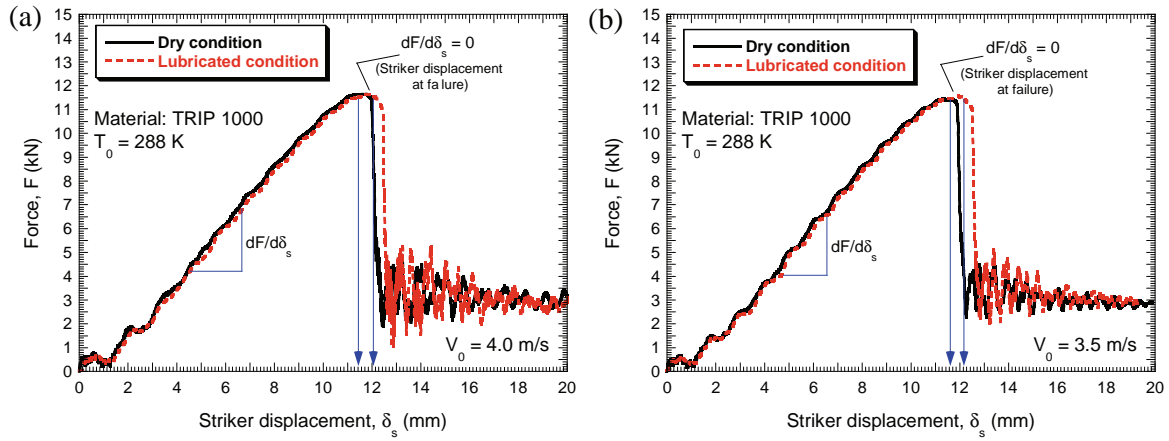
Fig. 21. Evolution of the impact force as a function of the striker displacement for both friction conditions. (a) $V_0 = 3.5$ m/s, (b) $V_0 = 4.0$ m/s.
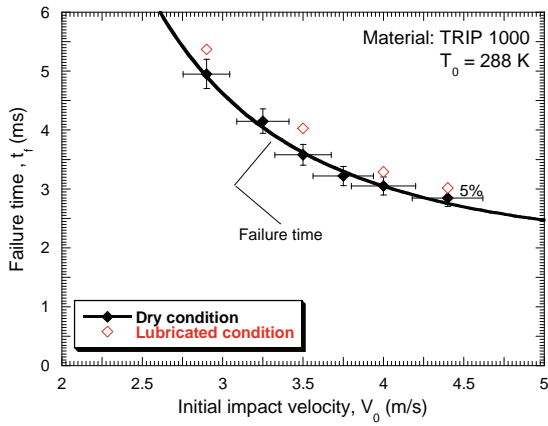

Fig. 22. Progression of the failure time as a function of the impact velocity for both friction conditions.

Therefore, in the case of lubricated contact the plate absorbs a larger amount of energy as plastic work, Fig. 24. The ballistic limit, which depends on the interface condition, is increased from $V_{bl}|_{dry} = 2.6$ m/s to $V_{bl}|_{lubricated} = 2.8$ m/s, as illustrated in Figs. 24 26.

The difference in the energy absorbed by the plate depending on the friction condition is illustrated in Figs. 25 and 26. For $V_0 = 2.9$ m/s the projectile hardly pierces the target in the case of lubricated contact, Fig. 25. However, in the case of dry contact and for the same impact velocity, several cracks precursor of *petal ling* can be observed, Fig. 26.

4.3. Effect of initial temperature

Finally, in this section the effect of the initial temperature on the perforation process is studied. The tests performed at $T_0 = 288$ K are compared to those conducted at $T_0 = 213$ K. The experiments at low temperature are carried out in order to pro mote *martensite* formation during loading. It should be noted that before testing at low temperature, the steel sheets (*already clamped and screwed*) were subjected to the testing temperature for 1 h. Such a period of time was considered as suitable in order to reach the thermal equilibrium of the system material target/testing temperature.

The first observation concerns the failure mode of the target. No influence of the initial temperature on the perforation mechanisms has been observed for the whole range of impact velocities consid ered. The final stage of the perforation process is the development of *petals*, as illustrated in Figs. 27 and 28.

However, the difference occurs with the energy absorbed by the target, as shown in Fig. 29. At low temperature the ballistic limit is
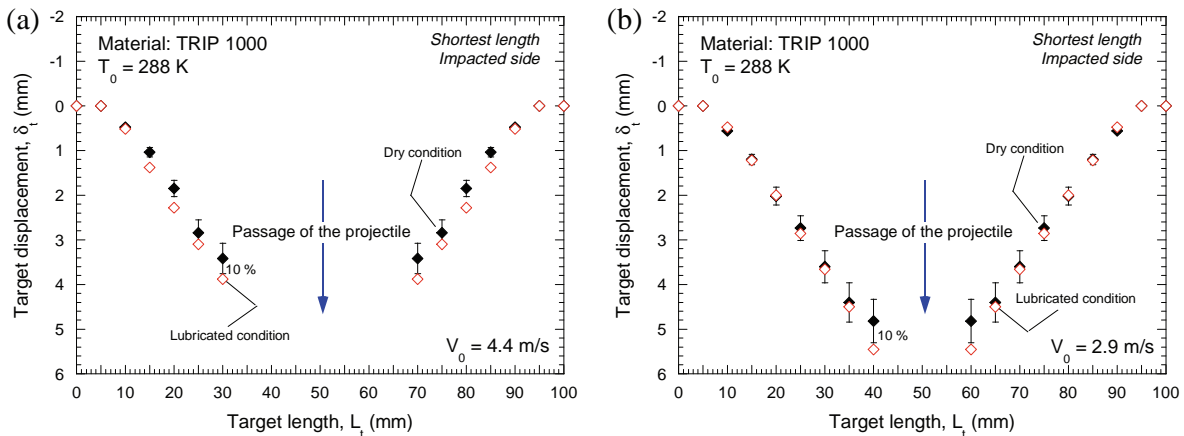

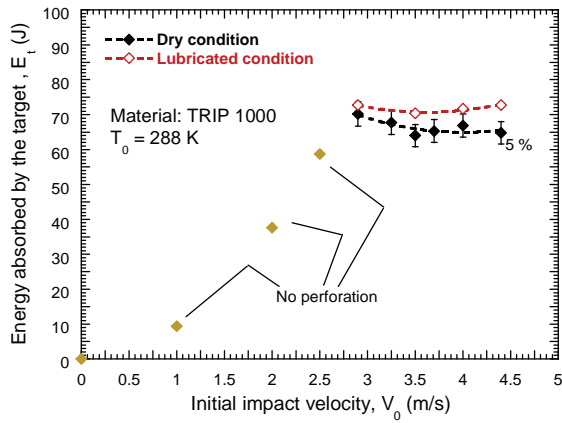**Fig. 23.** Target displacement for both friction conditions and different impact velocities.

Fig. 24. Energy absorbed by the target as a function of the impact velocity for dry and lubricated conditions.

increased from $V_{bl}|_{dry}^{T_0\ 213\,K}$ 2.6 m/s to $V_{bl}|_{dry}^{T_0\ 288\,K}$ 3.1 m/s, respectively.

For V_0 = 2.9 m/s and T_0 = 213 K the striker does not generate any cracks in the target, Fig. 30. However, it is shown in Fig. 26 that for the same impact velocity and T_0 = 288 K several cracks precursor of *petalling* occurred.

The plastic bending of the impacted specimens is larger at low temperatures, especially when the impact velocity is close to the ballistic limit, as demonstrated in Fig. 31. In the case of T_0 = 213 K, the target absorbs a larger amount of energy in the form of plastic work.

In Fig. 32 the progression of the striker velocity and the evolution of the loading time as a function of the striker displacement are shown for both initial temperatures and different impact velocities. The striker velocity during perforation as well as the loading time are not influenced by the initial temperature until target failure at T_0 = 288 K is reached, Fig. 32. Beyond that point the difference sets in Fig. 32.

Such a phenomenon has been observed in the progression of the impact force as a function of the striker displacement, as illustrated in Fig. 33. The force level at both initial temperatures is superimposed up to a determined value of the striker displacement. The testing temperature only affects the perforation process beyond certain deflection of the plate. Then, the difference resides in the slope of the curve force/striker displacement, Fig. 34.

In the following section, the potential *martensitic* transformation taking place during perforation process will be analyzed.
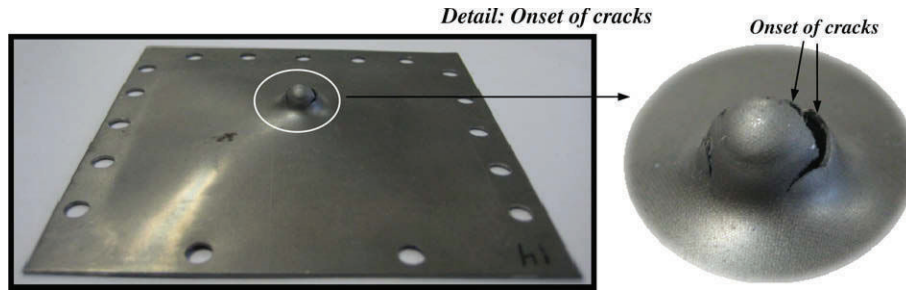

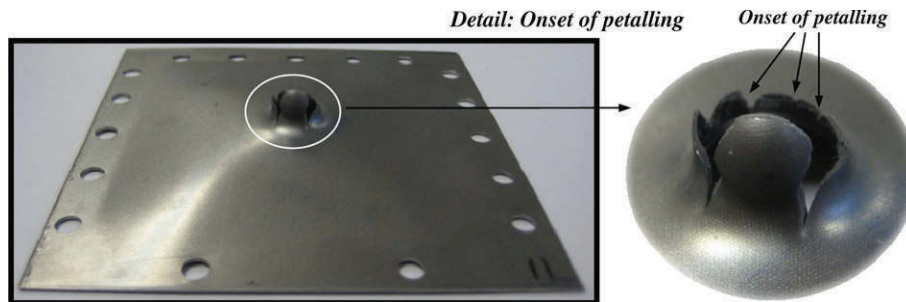**Fig. 25.** Petalling failure mode for V_0 = 2.9 m/s and T_0 = 288 K. Lubricated condition.

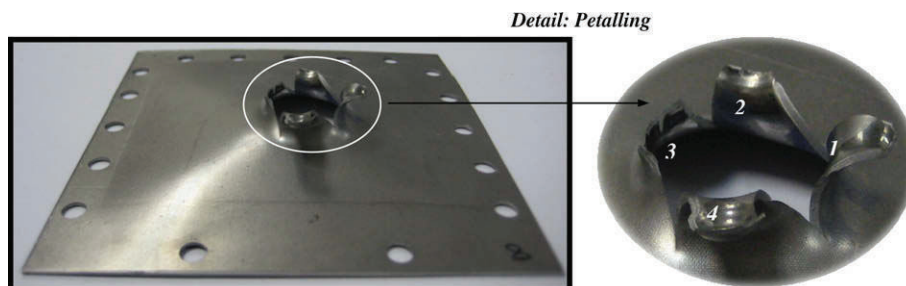**Fig. 26.** Petalling failure mode for V_0 = 2.9 m/s and T_0 = 288 K. Dry condition.

Fig. 27. Petalling failure mode for V_0 = 3.7 m/s and T_0 = 288 K. Dry condition.
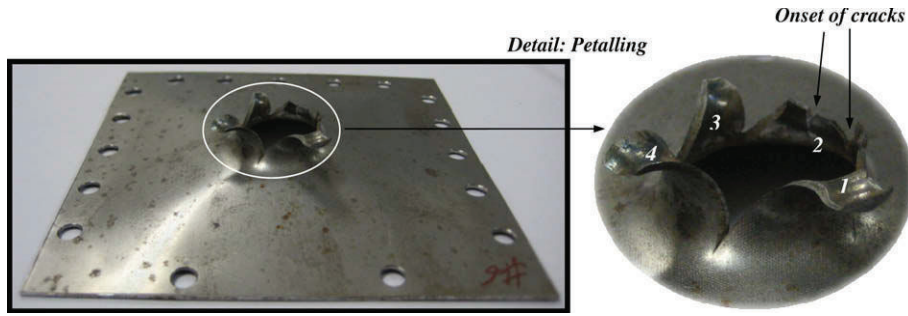
Fig. 28. Petalling failure mode for V_0 = 3.7 m/s and T_0 = 213 K. Dry condition.
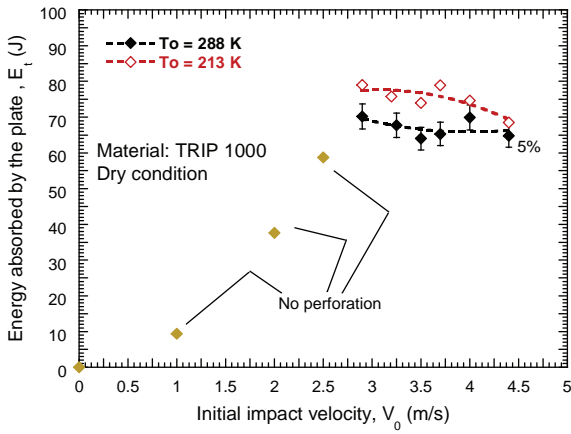

Fig. 29. Energy absorbed by the target in dependence on the impact velocity for T_0 = 288 K and T_0 = 213 K.

5. XRD analysis of the martensitic transformation during perforation

Since *martensitic* transformation is favoured with decreasing initial temperature, the plates impacted at T_0 = 213 K were analyzed by using XRD. The absence of phase transformation in this case would imply its absence at higher initial temperatures.

The volume fraction of the retained *austenite* has been determined at different points of the impacted specimens, especially close to the cracked interface. Flat petals have also been tested after cutting. The results revealed a volume fraction of retained *austenite* about 2% on the surface of the specimens after failure. The gradient detected along the thickness of 300 μm was still the same. This is the same amount of retained *austenite* observed before testing the samples. From this it is concluded that there is no *martensitic* transformation during perforation.

Close to the zone directly affected by the impact this absence of *martensite* may be explained by the increase in temperature during
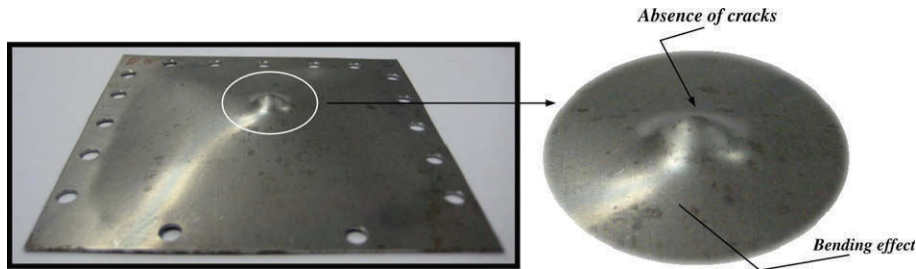

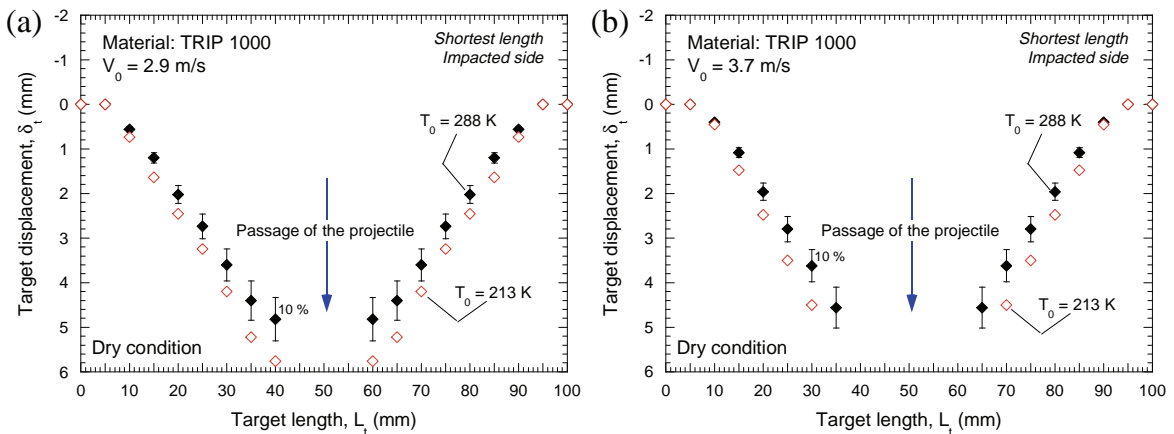**Fig. 30.** Petalling failure mode for V_0 = 2.9 m/s and T_0 = 213 K. Dry condition.

Fig. 31. Target displacement for both initial temperatures. (a) V_0 = 2.9 m/s, (b) V_0 = 3.7 m/s.
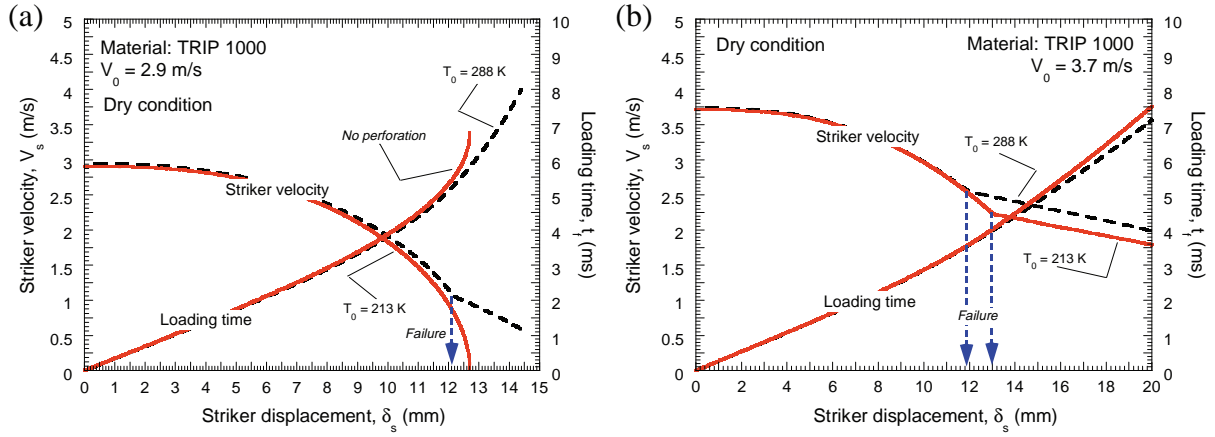
13

Fig. 32. Evolution of the striker velocity and of the loading time in dependence on the striker displacement for both initial temperatures. (a) $V_0 = 2.9$ m/s, (b) $V_0 = 3.7$ m/s.
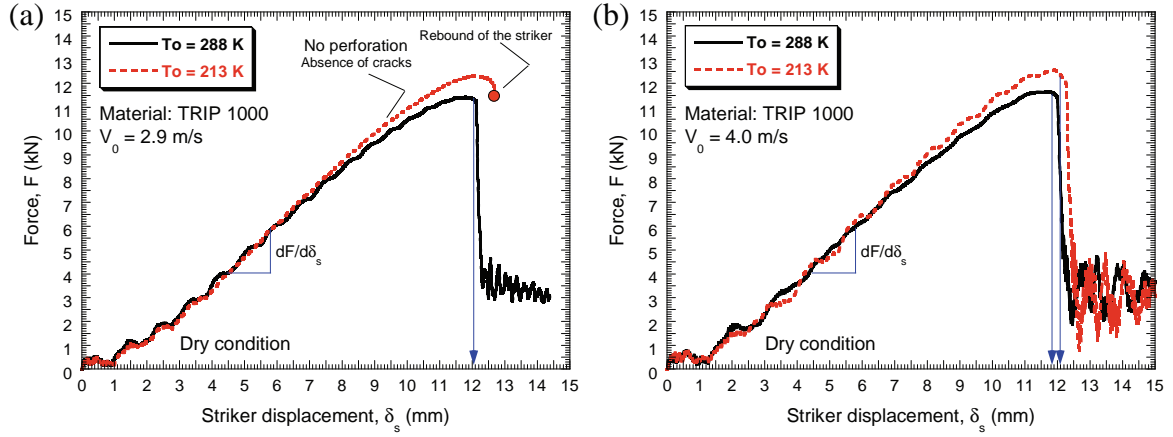

Fig. 33. Evolution of the force in dependence on the striker displacement for both initial temperatures. (a) $V_0 = 2.9$ m/s, (b) $V_0 = 4.0$ m/s.

dynamic loading. In fact, for TRIP 1000, the temperature increase of $\Delta T \approx 80$ K is already important under quasi static loading, as re ported by Rusinek and Klepaczko (2009). It is assumed that during perforation the local temperature (*close to the zone directly affected by the impact, austenite may be deformed*) deviates too much from the M_s temperature of this material. It makes the *austenite* phase stable even under potential large deformation in the *austenite*.

Moreover, a complete residual stress profile of the *ferrite* phase has also been recorded, in the longitudinal (LD) and transverse (TD) directions of the impacted plates referring to both radial and cir cumferential stresses, as illustrated in Fig. 35.

The stress values obtained for two impact velocities, $V_0 = 4$ m/s and $V_0 = 4.4$ m/s, are presented in Fig. 36. The results are shown as a function of the distance from the border of the specimen. This
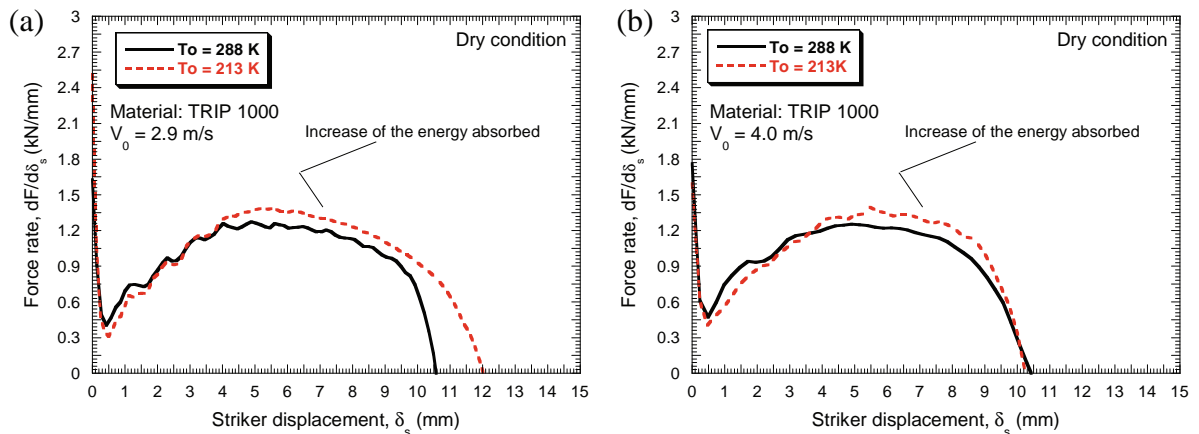

Fig. 34. Evolution of the force rate in dependence on the striker displacement for both initial temperatures. (a) $V_0 = 2.9$ m/s, (b) $V_0 = 4.0$ m/s.
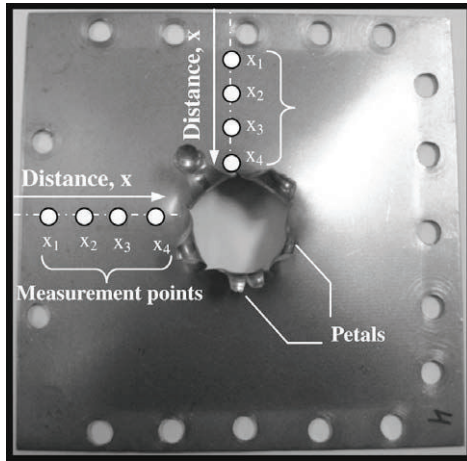
Fig. 35. Measuring points where the XRD technique was applied.

distance can slightly vary in both directions (LD and TD) depending on the shape of the perforated zone. It should be noted that some points close to the impacted zones could not be analysed because petals constitued obstacles to X rays.

Negative values of the residual stresses in *ferrite*, as illustrated in Fig. 36 a d, indicate that this phase is in the compressive state in TRIP 1000 (*play the role of soft phase*). *Cementite*, present in *bainite*, and *austenite* possess higher flow stresses (*play the role of hard phases*) in this steel. During loading, the stress in *ferrite* is therefore inferior in contrast to the superimposed macroscopic stress of the material. The main part of the plastic deformation re quired for the *austenite* to *martensite* formation is localized in the *ferrite*. In the target zones where an increase in temperature was not noticeable due to its remote position far from the zone directly affected by the impact, reduced deformation of the *austenite* phase seems to prevent *martensitic* transformation.

The radial stress values are maximum in *ferrite* close to the im pacted zones. There, the discrepancy between the macroscopic stress and the internal stress state in *ferrite* exhibits a maximum. This is because the amount of strain in *ferrite* is greater in the zone directly affected by the impact.

It must be noted that positive stress values in *ferrite* are ob served for the circumferential stress in the reduced range 28 mm $\leqslant X \leqslant$ 32 mm, as shown in Fig. 36b d. This local behaviour may be associated to the curvature changes in the profiles of the impacted plates. Since the samples tested have a square shape, the bending effect is not symmetric, either in the radial or in the circumferential direction. It should be noted that impact induces radial wave propagation; however, the distance to the clamped perimeter is not the same in all directions. In order to accommo date plastic deformation, the tested samples exhibit local tensile state (*in the circumferential direction*) in the previously mentioned target zone, 28 mm $\leqslant X \leqslant$ 32 mm.

6. Conclusions and remarks

This paper describes the thermo mechanical behaviour of TRIP 1000 steel sheets subjected to low velocity perforation by conical
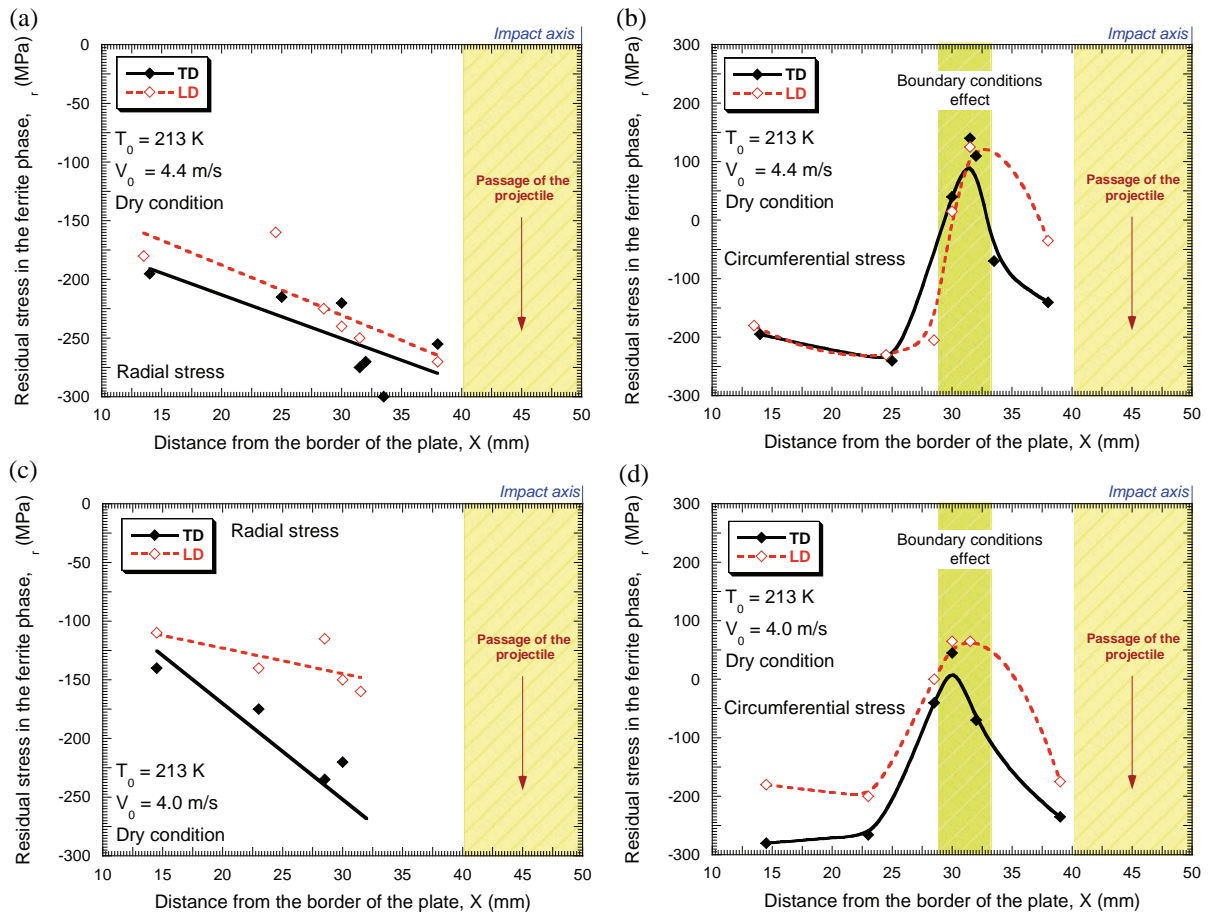

Fig. 36. Residual stress in ferrite in dependence on the distance from the border to the center of the plate for different initial impact velocities at T_0 = 213 K. (a) and (b) V_0 = 4.4 m/s, (c) and (d) V_0 = 4.0 m/s.

projectiles. A drop weight tower has been used to perform perfora tion tests at different impact velocities in the range $2.5\,\mathrm{m/s} \leqslant V_0 \leqslant 4.5\,\mathrm{m/s}$ at two initial temperatures: $T_0 = 213\,\mathrm{K}$ and $T_0 = 288\,\mathrm{K}$, respectively. Dry and lubricated friction contacts have been chosen for the striker/plate interactions. The stress distribu tion in the material as well as a *martensitic* transformation that might take place during perforation were evaluated by using X ray diffraction. The following main conclusions are drawn:

- In the range of the applied impact velocities and initial temper atures considered, *petalling* is the main failure mode of the per foration process. The number of the pronounced petals occurring in all tests performed varies between four and five. It should be noted that neither friction condition nor initial tem perature influences substantially the failure mechanisms.
- The perforation process is influenced by the type of contact. The target failure in the case of lubricated condition is delayed due to the absence of tangential stresses on the interface striker/ plate, $\mu \approx 0$. This circumstance reduces the localization of defor mation at the interface striker/target. Larger striker displace ment at failure leads to larger bending effect. The energy absorbed by the plate in lubricated conditions is larger than in the case of dry contact.
- A decreasing testing temperature leads to larger values of the impact energy absorption by the target. Plastic deformation by bending of the impacted specimens is greater at low tempera ture especially when the impact velocity is close to the ballistic limit. At $T_0 = 213\,\mathrm{K}$ the target absorbs large amounts of energy in the form of plastic work.
- However, it has been proven that the difference in the energy absorbed by the plates depending on the initial temperature is not caused by *martensitic* transformation but by temperature sensitivity of the material. XRD enables to measure the *austenite* content of the samples before and after the impact test. The results revealed the same volume fraction of *austenite*. The absence of *martensitic* transformation may be explained by the increase in temperature during loading in the zone affected by the impact. Moreover, residual stress analysis of *ferrite* showed that it plays the role of the soft phase during plastic deformation of the material. An important part of the plastic strain required for the *austenite* to *martensitic* transformation is localized in *fer rite*. In the target zones where an increase of temperature was not noticeable (*far from the zone directly affected by the impact*), reduced deformation of the *austenite* phase prevents *martensitic* transformation. Under these considerations (*including loading conditions*) TRIP 1000 steel seems to behave as a regular HSS with the absence of *martensitic* transformation.

In forthcoming studies it would be necessary to make progress in the analysis of the mechanisms that prevent *martensitic* trans formation in TRIP 1000 steel. A complete analytical description of the behavior of the coexisting phases of the material in the accom modation of plastic deformation during impact loading is required. Moreover, a detailed analysis of the influence of the loading path on the potential phase transformation of TRIP 1000 is necessary. In the case of dynamic loading processes, infrared measurements of the temperature increase on the material can be especially use ful to study the influence of adiabatic heating on *martensitic* transformation.

References

Al-Abbasi, F.M., Nemes, J.A., 2003. Micromechanical modeling of dual phase steels. Int. J. Mech. Sci. 45, 1449–1465.

Arias, A., Rodríguez-Martínez, J.A., Rusinek, A., 2008. Numerical simulations of impact behaviour of thin steel to cylindrical, conical and hemispherical non-deformable projectiles. Eng. Fract. Mech. 75, 1635–1656.

Borvik, T., Langseth, M., Hoperstad, O.S., Malo, K.A., 2002. Perforation of 12 mm thick steel plates by 20 mm diameter projectiles with flat, hemispherical and conical noses. Part I: experimental study. Int. J. Impact Eng. 27, 19–35.

Bouaziz, O., Guelton, N., 2001. Modelling of TWIP effect on work-hardening. Mater. Sci. Eng. A, 246–249.

Bouaziz, O., Allain, S., Scott, C., 2008. Effect of grain and twin boundaries on the hardening mechanisms of twinning induced plasticity steels. Scripta Mater. 58, 484–487.

Curtze, S., Kuokkala, V.T., Hokka, M., Peura, P., 2009. Deformation behavior of TRIP and DP steels in tension at different temperatures over a wide range of strain rates. Mater. Sci. Eng. A 507, 124–131.

Da Rocha, M.R., Silva de Oliveira, C.A., 2009. Evaluation of the martensitic transformations in austenitic stainless steels. Mater. Sci. Eng. A 517, 281–285.

Delannay, L., Jacques, P., Pardoen, T., 2008. Modelling of the plastic flow of trip-aided multiphase steel based on an incremental mean-field approach. Int. J. Solids Struct. 45, 1825–1843.

Fischer, F.D., Reisner, G., Werner, E., Tanaka, K., Cailletaud, G., Antretter, T., 2000. A new view on transformation induced plasticity (TRIP). Int .J. Plasticity 16, 723–748.

Greenwood, G.W., Johnson, R.H., 1965. The deformation of metals under small stresses during phase transformation. Proc. Roy. Soc. A 283, 403.

Hauk, V., 1997. Structural and Residual Stress Analysis by Nondestructive Methods. Elsevier, Amsterdam.

Huh, H., Seok-Bong Kima, S.B., Songa, J.H., Lim, J.H., 2008. Dynamic tensile characteristics of TRIP-type and DP-type steel sheets for an auto-body. Int. J. Mech. Sci. 50, 918–931.

Inal, K., Pesci, R., Lebrun, J.L., Diard, O., Masson, R., 2006. Grain and phase stress criteria for behaviour and damage in duplex and bainitic steels. Fatigue Fract. Eng. Mater. Struct. 29, 685–696.

Iwamoto, T., Tsuta, T., 2000. Computational simulation of the dependence of the austenitic grain size on the deformation behaviour of TRIP steels. Int. J. Plasticity 16, 791–804.

Iwamoto, T., Tsuta, T., Tomita, Y., 1998. Investigation on deformation mode dependence of strain-induced martensitic transformation in TRIP steels and modeling of transformation kinetics. Int. J. Mech. Sci. 40, 173–182.

Jiménez, J.A., Carsí, M., Ruano, O.A., Frommeyer, G., 2009. Effect of testing temperature and strain rate on the transformation behaviour of retained austenite in low-alloyed multiphase steel. Mater. Sci. Eng. A 508, 195–199.

Klepaczko, J.R., Rusinek, A., Rodríguez-Martínez, J.A., Pęcherski, R.B., Arias, A., 2009. Modelling of thermo-viscoplastic behaviour of DH-36 and Weldox 460-E structural steels at wide ranges of strain rates and temperatures, comparison of constitutive relations for impact problems. Mech. Mater. 41, 599–621.

Landkof, B., Goldsmith, W., 1993. Petalling of thin metallic plates during penetration by cylindro-conical projectiles. Int. J. Solids Struct. 21, 245–266.

Larour, P., Verleysen, P., Bleck, W., 2006. Influence of uniaxial, biaxial and plane strain pre-straining on the dynamic tensile properties of high strength sheet steels. J. Phys. IV 134, 1085–1090.

Larour, P., Rusinek, A., Klepaczko, J.R., Beck, W., 2007. Effects of strain rate and identification of material constants for three automotive steels. Steel Res. Int. 78, 348–358.

Lebedev, A., Kosarchuk, V., 2000. Influence of phase transformations on the mechanical properties of austenitic stainless steels. Int. J. Plasticity 16, 749–767.

Leblond, J.B., Devaux, J., Devaux, J.C., 1989. Mathematical modelling of transformation induced plasticity in steels – I. Case of ideal-plastic phases; II. Coupling with strain hardening phenomena. Int. J. Plasticity 5, 551–573.

Liu, J-Y., Lu, H., Chen, J-M., Jullien, J-F., Wub, T., 2008. Simulation of mechanical behavior of multiphase TRIP steel taking account of transformation-induced plasticity. Comput. Mater. Sci. 43, 646–654.

Magee, C.L., 1966. Transformation kinetics, micro-plasticity and aging of martensite in Fe–31 Ni. Ph.D. Thesis, Carnegie Institute of Technology, Pittsburgh, PA.

Meftah, S., Barbe, L., Taleb, L., Sidoroff, F., 2007. Parametric numerical simulations of TRIP and its interaction with classical plasticity in martensitic transformation. Eur. J. Mech. A/Solids 26, 688–700.

Oliver, S., Jones, T.B., Fourlaris, G., 2007. Dual phase versus TRIP strip steels: microstructural changes as a consequence of quasi-static and dynamic tensile testing. Mater. Charact. 58, 390–400.

Papatriantafillou, I., Agoras, M., Aravas, N., Haidemenopoulos, G., 2006. Constitutive modeling and finite element methods for TRIP steels. Comput. Methods Appl. Mech. Eng. 195, 5094–5114.

Pesci, R., Inal, K.R., Masson, R., 2009. A three scale polycrystalline modeling of behavior of a 16MND5 bainitic steel: stress distribution at low temperatures. Mater. Sci. Eng. A 527, 376–386.

Rodríguez-Martínez, J.A., Rusinek, A., Zaera, R., Arias, A., Klepaczko, J.R., 2008. Estudio experimental y numérico del comportamiento de láminas de acero sometidas a impacto de media y alta velocidad. Anales de Mecánica de la fractura (in Spanish).

Rodríguez-Martínez, J.A., Rusinek, A., Klepaczko, J.R., Pecherski, R.B., 2009. Extension of R–K constitutive relation to phase transformation phenomena. J. Mater. Design 30, 2513–2520.

Rusinek, A., Klepaczko, J.R., 2009. Experiments on heat generated during plastic deformation and stored energy for TRIP steels. Mater. Des. 30, 35–48.

Rusinek, A., Rodríguez-Martínez, J.A., Arias, A., Klepaczko, J.R., López-Puente, J., 2008. Influence of conical projectile diameter on perpendicular impact of thin steel plate. Eng. Fract. Mech. 75, 2946–2967.

Rusinek, A., Rodríguez-Martínez, J.A., Klepaczko, J.R., Pecherski, R.B., 2009a. Analysis of thermo-visco-plastic behaviour of six high strength steels. J. Mater. Des. 30, 1748–1761.

Rusinek, A., Rodríguez-Martínez, J.A., Zaera, R., Klepaczko, J.R., Sauvelet, C., Arias, A., 2009b. Experimental and numerical analysis of failure process of mild steel sheets subjected to perpendicular impact by hemispherical projectiles. Int. J. Impact Eng. 36, 565–587.

Sanchez-Saez, S., Barbero, E., Navarro, C., 2007. Analysis of the dynamic flexural behaviour of composite beams at low temperature. Compos. Sci. Technol. 67, 2616–2632.

Taleb, L., Petit, S., 2006. New investigations on transformation induced plasticity and its interaction with classical plasticity. Int. J. Plasticity 22, 110–130.

Tomita, Y., Iwamoto, T., 1995. Constitutive modelling of TRIP steel and its application to the improvement of mechanical properties. Int. J. Mech. Sci. 37, 1295–1305.

Wierzbicki, T., 1999. Petalling of plates under explosive and impact loading. Int. J. Impact Eng. 22, 935–954.